Available online at www.sciencedirect.com
ScienceDirect
Energy 32 (2007) 1343–1351
ENERGY
www.elsevier.com/locate/energy

Optimized mass flux ratio of double-flow solar air heater with EHD

N. Kasayapanand[a,*], T. Kiatsiriroat[b]

[a]School of Energy, Environment, and Materials, King Mongkut's University of Technology Thonburi, Bangkok 10140, Thailand
[b]Department of Mechanical Engineering, Chiang Mai University, Chiang Mai 50200, Thailand

Received 25 March 2006

Abstract

The numerical study of laminar forced convection inside double-flow solar air heater with electrohydrodynamic technique is investigated by finite difference method. The electric field is generated by the wire electrodes charged with DC high voltage. The mathematical modeling of computational fluid dynamics includes the interactions among electric field, flow field, and temperature field. It can be perceived that augmented heat transfer with presence of an electric field increases with the supplied voltage but decreases with the total mass flux. The optimized mass flux ratio is expressed incorporating with concerning parameter comprising of the electrode arrangement, the number of electrodes, the total heat flux at an absorbing plate, and the channel geometry.

Keywords: Electrohydrodynamic; Computational fluid dynamics; Solar air heater; Heat transfer enhancement

1. Introduction

A flat plate solar air heater is equipment that converts solar energy into heat for generating hot air. It consists of one or more sheets of glass or transparent material situated above an absorbing plate where the air is flowing either over or under along the plate. To achieve a considerable improvement in collector efficiency, some techniques to extend the area of the absorbing plate or adjust the flow configuration have been carried out. Satcunanathan and Deonarine [1] constructed a two-pass air heater in which the air flows through the glass pane before passing through the blackened metal absorber plate. A set of performance curves of the solar air heater with two-pass flow arrangements were also developed by Wijeysundera et al. [2]. Yeh et al. [3,4] investigated experimentally and theoretically collector efficiency of double-flow solar air heaters. The double-flow device creates the solar collector with double heat transfer area between the absorbing plate and the heated air; this advantage might compensate the heat loss from the top thus high performance is obtained.

The enhancement technique utilizing electrostatic force generated from the polarization of dielectric fluid can be one of the most promising methods among various active techniques for enhancing the heat transfer between the absorbing plate and the heated air with small consumptions of electrical power. This technique is frequently called electrohydrodynamic (EHD) method of heat transfer, which refers to the interdisciplinary field. There are some studies relating to the EHD, for instances, Yabe et al. [5] investigated the phenomenon of a corona wind between wire and plate electrodes, which increases heat transfer at the wall surface under natural convection. Velkoff and Godfrey [6] indicated the heat transfer enhancement over a horizontal flat plate with parallel wire electrodes. This characteristic was confirmed again by Yamamoto and Velkoff [7] who investigated the computational method in electrostatic precipitator. Tada et al. [8] unveiled the fundamental mechanism of heat transfer augmentation in a two-dimensional rectangular duct. Kasayapanand et al. [9] investigated the numerical results of the effect of electrode arrangements in tube bank on the heat transfer enhancement characteristics. Kasayapanand and Kiatsiriroat [10] conducted numerically augmented heat transfer coefficient of air flow inside wavy channel with several electrode arrangements. Recently, Kasayapanand and

*Corresponding author. Tel./fax: +66 0 2470 8699; fax: +66 0 2427 9062.
E-mail address: nat.kas@kmutt.ac.th (N. Kasayapanand).

0360-5442/$ - see front matter © 2006 Elsevier Ltd. All rights reserved.
doi:10.1016/j.energy.2006.11.001

Nomenclature

c_p	specific heat, J/kg K
D_e	charge diffusion coefficient, $m^2/V\,s$
$\boldsymbol{E}$	electric field strength, V/m
$\boldsymbol{F}_E$	electrohydrodynamic body force, N/m^3
$\boldsymbol{g}$	acceleration due to gravity, m/s^2
h	heat transfer coefficient, $W/m^2\,K$
H	channel height, m
$\boldsymbol{J}$	current density, A/m^2
k	thermal conductivity, W/m K
L	length of computational domain, m
m	total mass flux, kg/s
n	normal direction to the surface
Nu	Nusselt number (with electric field)
Nu_0	Nusselt number (without electric field)
P	pressure, N/m^2
Pr	Prandtl number
Re	Reynolds number
q_c	electric charge density, C/m^3
q	heat flux at an absorbing plate, W/m^2
t	time, s
T	temperature, K
U_i	inlet air velocity, m/s
$\boldsymbol{v}$	fluid velocity, m/s
V	voltage, V

Greek symbols

α	thermal diffusivity, m^2/s
β	volume expansion coefficient, 1/K
ε	fluid permittivity, F/m
η	thermal collector efficiency
μ	dynamic viscosity, kg/m s
v	kinematic viscosity, m^2/s
ρ	density, kg/m^3
σ_e	electrical conductivity, 1/ohm m
$\boldsymbol{\omega}$	vorticity, 1/s
ψ	stream function, m2/s

Subscripts

0	at wire electrode
a	ambient
g	glass
L	lower sub-channel
U	upper sub-channel
m	mean value
w	wall surface

Kiatsiriroat [11] studied numerically and experimentally the optimum electrode arrangement of a single-flow solar air heater. The heat rate could get more heat nearly 100 W at low Reynolds number and the solar radiation around 900 W/m^2 while the electrical power supply for the EHD was consumed only about 0.5 W.

This numerical study conducts the mechanisms of EHD by considering electrostatic forces exerting to an air flowing inside the double-flow solar air heater configuration. Two-dimensional governing equations of the EHD phenomena and the corresponding boundary conditions are formulated. The mathematical modeling has been carried out to investigate the EHD enhanced flow and heat transfer. The wire electrodes charged with DC high voltage are placed perpendicular to the flow direction. The interactions of electric field, flow field, and temperature field are discussed in conjunction with the parameters comprising of the total mass flux, the mass flux ratio, the supplied voltage, the electrode arrangement, the number of electrodes, the heat flux at an absorbing plate, and the channel geometry.

2. Theoretical analysis

The governing equations for the EHD force per unit volume $\boldsymbol{F}_E$ generated by the electric field with strength $\boldsymbol{E}$ in a fluid of dielectric permittivity ε, electric charge density q_c, density ρ, and uniform temperature T can be expressed as [12]

$$\boldsymbol{F}_E = q_c\boldsymbol{E} - \frac{1}{2}\boldsymbol{E}^2\nabla\varepsilon + \frac{1}{2}\nabla\left[\boldsymbol{E}^2\left[\frac{\partial\varepsilon}{\partial\rho}\right]_T\rho\right]. \tag{1}$$

The first term of the right is the Coulomb force exerted by electric field upon the free charge or electrophoretic component. The second and the third terms correspond to the dielectrophoretic and electrostrictive forces on and within the fluid. Eq. (1) is then included in the Navier–Stokes equation, by assuming incompressible fluid, the conservation of momentum is given by

$$\rho\frac{\mathrm{d}v}{\mathrm{d}t} = \rho\boldsymbol{g} + F_E - \nabla P + \mu\nabla^2\boldsymbol{v}. \tag{2}$$

The vector $\rho\boldsymbol{g}$ is the gravitational force per unit volume, P is the local fluid pressure and the last term in the right-hand side of equation represents the viscous terms. Introducing the vorticity $\boldsymbol{\omega}$ as

$$\boldsymbol{\omega} = \nabla\times\boldsymbol{v}. \tag{3}$$

To get the vorticity transport equation in two-dimensional flow, the momentum equation can be rewritten in terms of the vorticity defined above, so that

$$\frac{\partial\boldsymbol{\omega}}{\partial t} + (\boldsymbol{v}\cdot\nabla)\boldsymbol{\omega} = v\nabla^2\boldsymbol{\omega} - \boldsymbol{g}\beta\frac{\partial\mathrm{T}}{\partial x} - (\boldsymbol{E}\times\nabla)q_c. \tag{4}$$

The stream function (ψ) for two-dimensional problems is defined such that

$$\boldsymbol{v} = \nabla\times(\psi\boldsymbol{e}_z), \tag{5}$$

vorticity transport equation can be obtained from Eqs. (4) and (5) further gives

$$\nabla^2\psi = -\boldsymbol{\omega}. \tag{6}$$

The energy equation of this system, without viscous dissipation effect, can be written as

$$\frac{\mathrm{d}T}{\mathrm{d}t} = \alpha\nabla^2 T + \frac{\sigma_e \boldsymbol{E}^2}{\rho c_p}. \tag{7}$$

The above equations could be applied for the solar air heater as shown in Fig. 1. The appropriate and sufficient boundary conditions for the flow and the temperature fields of the double-flow system as shown in Fig. 2 are given by

$$x = 0(\text{upper}); \quad \boldsymbol{\omega} = 0, \quad \psi = HU_i\left(1 - \frac{m_U}{m_{Total}}\right) + \frac{m_U U_i}{m_{Total}}\left(\frac{2y}{H} - 1\right), \quad T = T_i, \tag{8a}$$

$$x = 0(\text{lower}); \quad \boldsymbol{\omega} = 0, \quad \psi = 2yU_i\left(1 - \frac{m_U}{m_{Total}}\right), \quad T = T_i, \tag{8b}$$

$$x = L; \quad \frac{\partial\omega}{\partial x} = 0, \quad \frac{\partial\psi}{\partial x} = 0, \quad \frac{\partial^2 T}{\partial x^2} = 0, \tag{8c}$$

$$y = 0; \quad \boldsymbol{\omega} = -\frac{\partial^2\psi}{\partial y^2}, \quad \psi = 0, \quad \frac{\partial T}{\partial y} = 0, \tag{8d}$$

$$y = \frac{H}{2}(\text{upper}); \quad \omega = -\frac{\partial^2\psi}{\partial y^2}, \quad \psi = HU_i\left(1 - \frac{m_U}{m_{Total}}\right), \quad -k\frac{\partial T}{\partial y} = q_U, \tag{8e}$$

$$y = \frac{H}{2}(\text{lower}); \quad \boldsymbol{\omega} = -\frac{\partial^2\psi}{\partial y^2}, \quad \psi = HU_i\left(1 - \frac{m_U}{m_{Total}}\right), \quad k\frac{\partial T}{\partial y} = q_L, \tag{8f}$$

$$y = H; \quad \boldsymbol{\omega} = -\frac{\partial^2\psi}{\partial y^2}, \quad \psi = U_i H, \quad T = T_g, \tag{8g}$$

at the channel exit, the gradients of stream function, vorticity, and heat flux are set to zero. In addition to the conditions above, a uniform flow is specified at the inlet boundary as well as the non-slip and the constant summation of heat flux ($q_U + q_L$) conditions are employed along the absorbing plate.

Maxwell equations for the electric field corresponding to the setup are as follows:

$$\nabla \cdot \varepsilon\boldsymbol{E} = q_c, \tag{9}$$

the electric field strength $\boldsymbol{E}$ is given by

$$\boldsymbol{E} = -\nabla V. \tag{10}$$

As the current is conserved over the domain of calculation, the current continuity equation is represented as

$$\nabla \cdot \boldsymbol{J} + \frac{\partial q_c}{\partial t} = 0, \tag{11}$$

where the current density $\boldsymbol{J}$ is given by

$$\boldsymbol{J} = q_c\boldsymbol{v} + \sigma_e\boldsymbol{E} + (\boldsymbol{v}\cdot\nabla)(\varepsilon\boldsymbol{E}) - D_e\nabla q_c. \tag{12}$$

Combining Eqs. (9)–(12), one can obtain

$$\nabla^2 V = -\frac{q_c}{\varepsilon}, \tag{13}$$

$$q_c^2 = \varepsilon(\boldsymbol{E}\cdot\nabla q_c). \tag{14}$$

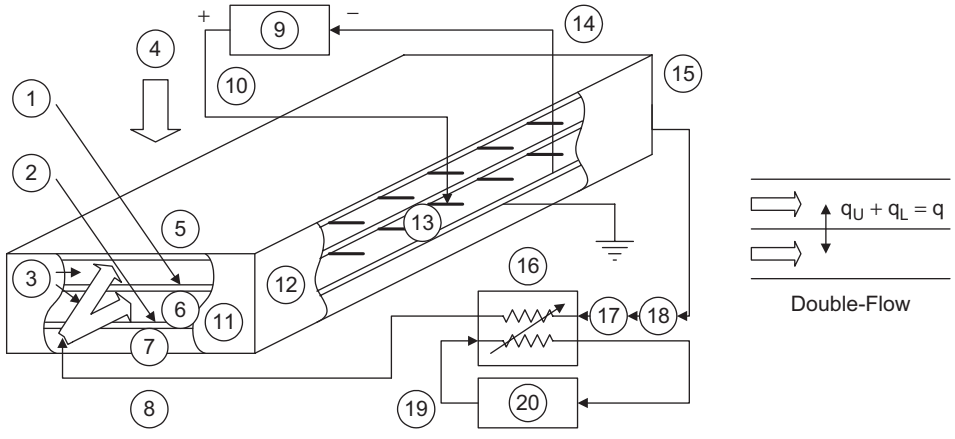

1. Absorbing Plate
2. Reflecting Sheet
3. Air Gap
4. Solar Heating
5. Glass Cover Plate
6. Air Flow Channel
7. Insulation
8. Inlet Air
9. High Voltage Generator
10. Positive Electrode
11. Insulation
12. Insulation
13. Wire Electrode
14. Grounded Electrode
15. Outlet Air
16. Heat Exchanger
17. Blower
18. Invertor
19. Working Fluid
20. Applications

Fig. 1. Schematic sketch of the double-flow solar air heater with EHD.

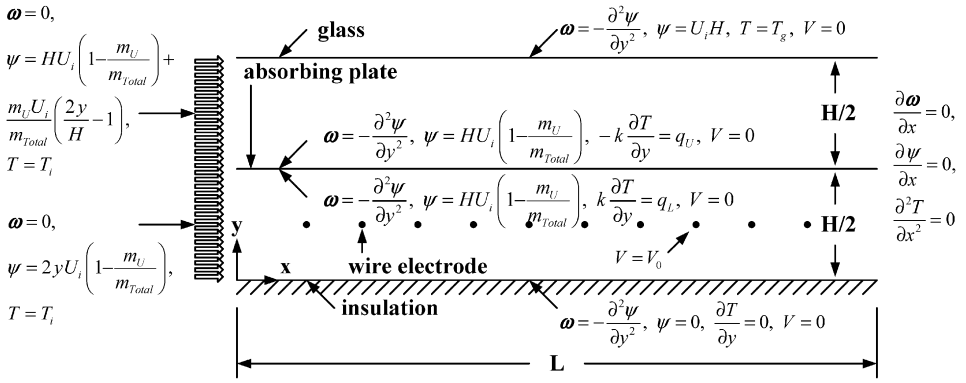

Fig. 2. Computational domain and boundary conditions of double-flow solar air heater.

The boundary conditions required for solving Eqs. (13) and (14) are

$$V = V_0, \text{ at the wire electrodes,} \tag{15a}$$

$$V = 0, \text{ along the wall surface.} \tag{15b}$$

In terms of heat transmission characteristic, the local heat transfer coefficient in term of the local Nusselt number of laminar sublayer near the surface is simply given by

$$Nu_x = \frac{2Hh}{(H+2)k} = \frac{2H(\partial T/\partial n)}{(H+2)(T_w - T_m)}, \tag{16}$$

Average heat transfer coefficient along the horizontal surface of channel can be determined such that

$$Nu = \frac{2H}{(H+2)L}\int_0^L \frac{(\partial T/\partial n)}{(T_w - T_m)}\mathrm{d}x. \tag{17}$$

The collector efficiency in this study is calculated from the heat rate absorbed by the air flow divided by the heat absorbed at an absorber plate.

3. Methodology

The schematic sketch of an EHD solar air heater apparatus is represented in Fig. 1. An absorbing plate divides the air duct into two equivalent channels. The configuration of air flow in the solar air heater considered in this simulation study is double-flow which the air is flowing over and under the absorbing plate. The effect of EHD on heat transfer enhancement of the solar air heater with this flow configuration is considered to determine the optimized mass flux ratio of various operating conditions. The illustration of computational domain and boundary conditions of double-flow configuration is shown in Fig. 2. The solar air heater dimensions comprise $L = 2.00$ and $H = 0.10\,\mathrm{m}$. The absorbing plate is maintained at a uniform heat flux between 200 and $1000\,\mathrm{W/m^2}$ (assuming that channel width is 1 m). The upper plate which is a glass pane has a uniform temperature of $T_g = 300\,\mathrm{K}$ and the lower plate which is the collector casing is insulated, all of the plates are electrically grounded. Air at a uniform velocity U_i and temperature $T_i = 300\,\mathrm{K}$ is introduced at the inlet. All electrode arrangements are installed at the middle position of the channels. The side loss is assumed to be negligible.

This study conducts grid generation method to convert the physical plane in Cartesian coordinates (x, y) into the computational plane in curvilinear coordinates (ξ, η) by Poisson's equation. The example of two types of mesh arrangement is illustrated in Fig. 3. For an electric field calculation as shown in Fig. 3(a), the first radial discrete value is computed using geometrical progression to allow high nodal density near the wire and the remaining region being subdivided into equispaced nodes. For greater distance from the wire, the circular symmetry changes gradually and fits into Cartesian reference at the grounded plates and the symmetrical axes between electrodes. The obtained electric charge and electric potential distributions are mapping into computational fluid dynamics grid arrangement for calculate the velocity and temperature fields in Fig. 3(b). All equations are non-dimensionalized and the numerical calculation could be carried out with the computational grids (1601×81) and a non-dimensional time step of 1×10^{-4} to ensure the numerical stability and accuracy. Since the radius of the wire electrode ($1 \times 10^{-4}\,\mathrm{m}$) is sufficiently small in the comparison to the grid spacing. Therefore, it is allowable to treat the wire as a nodal point. Several models have been proposed for the calculation of the electric field and charge density distribution in a wire–plate precipitation system using finite difference method [13–15]. The detail of the calculation procedure is as follows: Firstly, we assume q_{c0} at the wire electrode according to the semi-empirical formula by Peek [16]. The electric potential and electric charge density distribution are obtained responding to Eqs. (13) and (14) by upwind difference schemes and successive under relaxation method. The obtained values are employed to calculate electric current density at the grounded plate and compared to the initial value until convergence. Embarking an upwind difference scheme on velocity field at all nodes, the vorticity at each time step is hence obtained from Eq. (4), in accordance with the electric field and the stream function obtained from Eq. (6). The temperature field is finally acquired from Eq. (7). The above mentioned

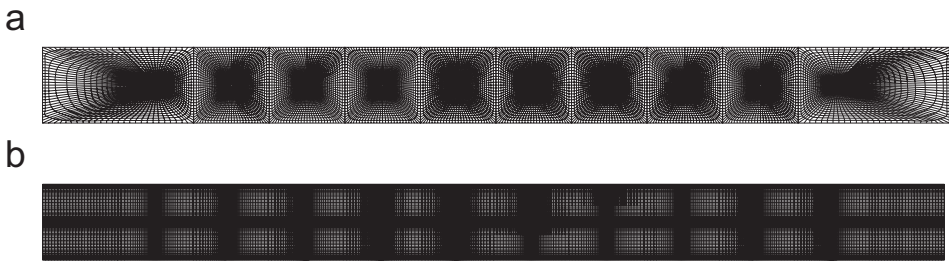

Fig. 3. Grid generations.

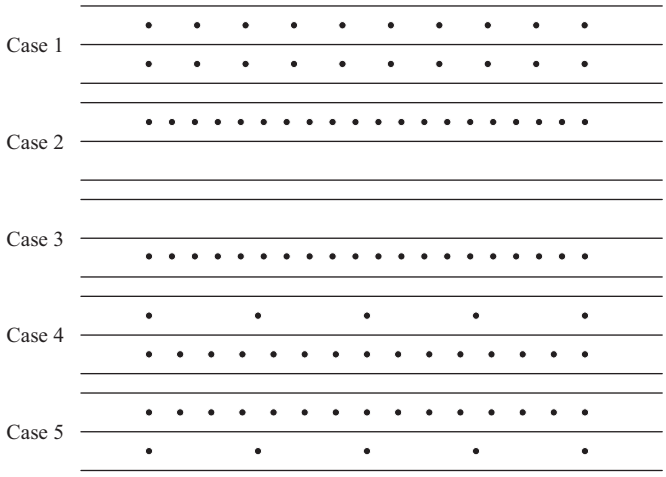

Fig. 4. Various categories of electrode arrangement.

procedures are repeated until the convergence of stream function and temperature are reached. The convergence criterion is selected when the results are in steady state or oscillatory state.

4. Results and discussion

For study the effect of EHD enhanced heat transfer in double-flow operation, five categories of electrode arrangement have been performed while the number of electrodes is fixed at twenty. In case 1, the upper and the lower channels each has 10 wire electrodes. Cases 2 and 3 have 20 electrodes installed only in one channel, upper and lower, respectively. Cases 4 and 5 have unequal electrodes of which the numbers are 15 and 5 in both channels. All the cases, the distance between electrodes is uniformly distributed along the channel length in the small scale of channel length ($L = 0.75$ and $H = 0.10$ m). Fig. 4 investigates the EHD applying with the electrode arrangements in cases 1–5 which have the same mass flux ($Re = 100$ based on characteristic length of $4\times$ cross-sectional area/perimeter in both sub-channels or $m_{Total} = 7.49$ kg/h). The stream lines of these categories are shown in Fig. 5. In case 1, there is a set of rotating cellular motions at all electrodes. Similarly results are found in cases 2 and 3 in the channel that has electrodes. Since the number of electrodes is rather high in these two cases, it is found that

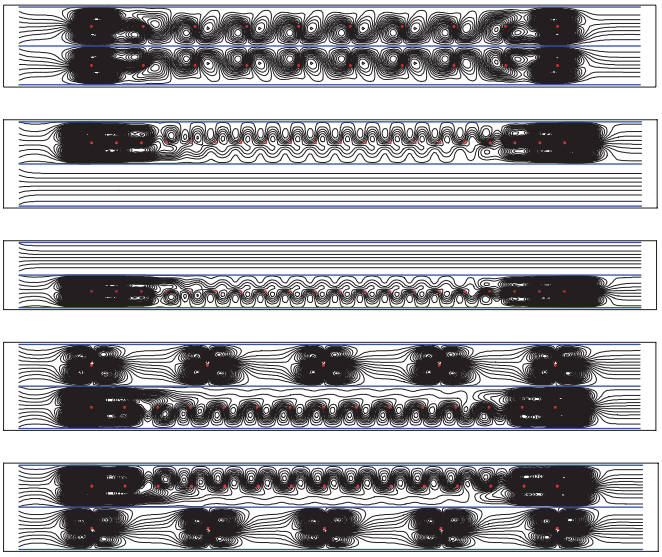

Fig. 5. Stream function contours in the double-flow solar air heater ($V_0 = 17.5$ kV, $m_{Total} = 7.49$ kg/h, and $m_U/m_{Total} = 50\%$).

there are many vortices around the electrodes and the flow patterns are oscillating due to the high density of an electric field. For the opposite channel that has no electrode, the stream lines pattern is similarly to laminar flow in a conduit. In cases 4 and 5, the effect of unequal electrode density causes different numbers of vortices occurs along both channels. It is found that the number of vortices increases in relation with the number of electrodes.

Fig. 6 shows the temperature distributions of the previous figure ($q = 1000$ W/m^2). A comparison of the collector efficiency of each category is investigated in Fig. 7. The isotherm lines density over and under the absorbing plate is found to be higher than the other cases that causes highest heat transfer coefficient in case 1. Since high heat transfer coefficient is obtained in the upper channel, therefore, high heat loss also occurs at the glass pane then the collector efficiency is not the highest. In cases 2 and 3, it is found that when the number of electrodes is too high even though there is a good turbulent mixing, but the flows are recirculating around the middle zone of the heating plate then lower heat transfer rates are obtained compared with the previous case. For case 2, when the flow is recirculating in the upper channel there is a high heat loss at the glass pane then the collector efficiency is the poorest.

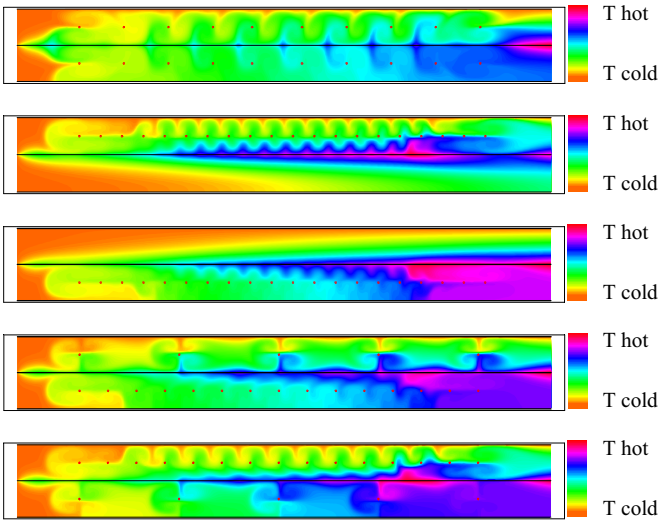

Fig. 6. Temperature distributions in the double-flow solar air heater ($V_0 = 17.5$ kV, $m_{Total} = 7.49$ kg/h, $m_U/m_{Total} = 50\%$, and $q = 1000$ W/m^2).

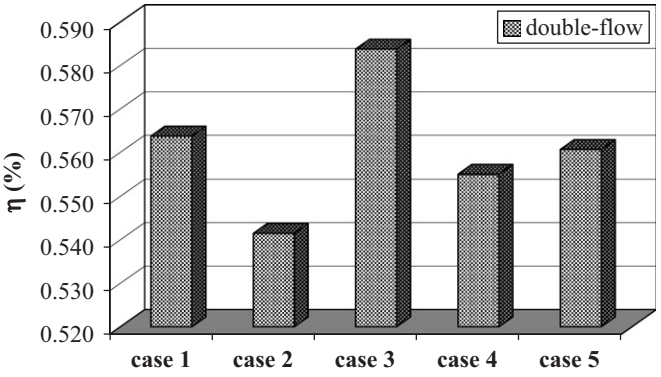

Fig. 7. Collector efficiency with different electrode arrangements ($V_0 = 17.5$ kV, $m_{Total} = 7.49$ kg/h, $m_U/m_{Total} = 50\%$, and $q = 1000$ W/m^2).

For case 3, poor heat transfer is obtained at the upper channel that has no electrode thus the heat loss is also small and the collector efficiency is highest. In case 4, the heat transfer is rather poor in the lower channel due to the high number of electrodes that generates a lot of recirculating vortices, and in the upper channel the heat transfer to the air is good that also conducts the heat loss to the glass pane, therefore, the collector efficiency is less than those in cases 1 and 3. In case 5, the efficiency slightly higher than that in case 4 even there is a low heat loss at the upper channel due to a lot of vortices formed by the high number of electrodes and at the lower channel the heat transfer from the absorber plate to the air is better. Fig. 8 demonstrates the augmented ratio of Nusselt number of various Reynolds numbers and supplied voltages. Higher the supplied voltage results in better heat transfer improvement and the electric field can enhances heat transfer significantly at low Reynolds number. For high velocity, the primary forced convection dominates the heat transfer. It can be noticed that when attention is brought

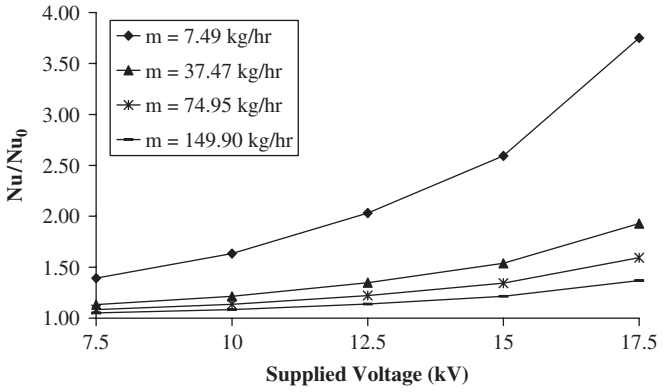

Fig. 8. Enhanced ratio of each mass flux ($m_U/m_{Total} = 50\%$ and $q = 1000$ W/m^2).

onto the extra received heat transfer of air per electrical power consumption, it is found that this ratio is varied in the range of 5–30 in this study which found to be very profitable.

Fig. 9 conducts the stream function contours of double-flow EHD solar air heater in case 3 of electrode arrangement which has different numbers of electrodes (this electrode arrangement performs the maximum thermal efficiency from Fig. 7). It can be seen that the many vortices occur around the wire electrodes at lower channel when the number of electrodes is increased. Fig. 10 shows the temperature distributions inside the solar air heater. It can be observed that at $N = 18$ (or ratio between distance between wire electrodes and sub-channel height = 1) has highest temperature gradient at the absorbing plate, which yields best performance for convective heat transfer. Considerable more improvement in collector efficiency is obtained by employing the optimum mass flux ratio between upper and total (upper + lower). At the low mass flux ratio, low mass flux at the upper channel leads to low heat loss at the glass pane that cause high average outlet temperature and high mass flux at the lower channel perceives slightly high collector efficiency, which is similarly to single-flow operation with air flow under an absorbing plate. Nevertheless, while the mass flux ratio increases, high heat loss occurs at the glass pane, but the heat transfer received on the upper channel is augmented while the lower channel is reduced. Therefore, the optimum condition must be occurring between two extreme boundaries when the total mass flux is fixed. The numerical results show that the optimum fraction of mass flow rate ratio for maximum collector efficiency in non-EHD is approximately to 0.5 for all operating conditions. It means that in order to achieve the best thermal performance of a double-flow solar air heater with non-EHD, in which the cross-sectional areas of upper and lower channels are equally constructed, the mass flow rates in both flow channels must be kept the same. A non-qualitative agreement is obtained between the EHD and Non-EHD results. The maximum collector efficiency with EHD (which has electrode arrangement in case 3) shifts into

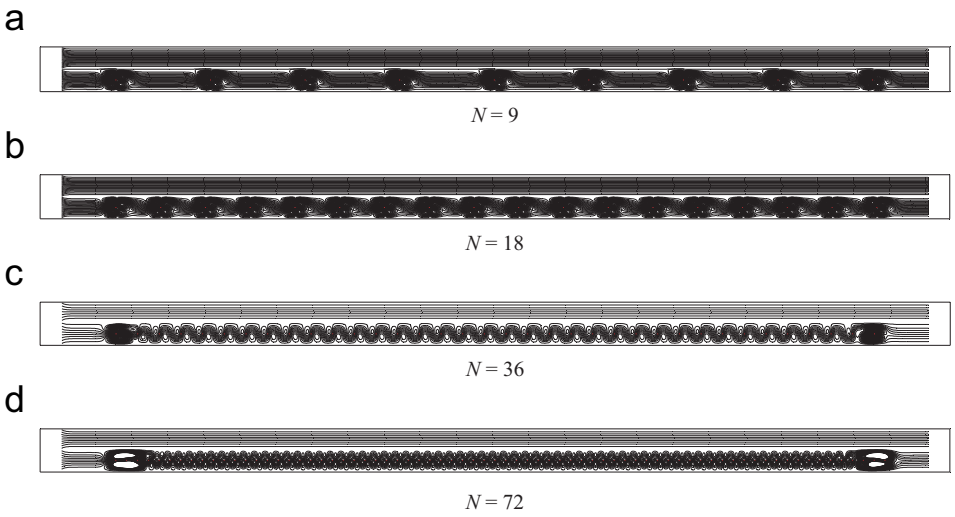

Fig. 9. Stream function contours of various number of electrodes ($V_0 = 17.5\,\text{kV}$, $m_{Total} = 7.49\,\text{kg/h}$, and $m_U/m_{Total} = 50\%$).

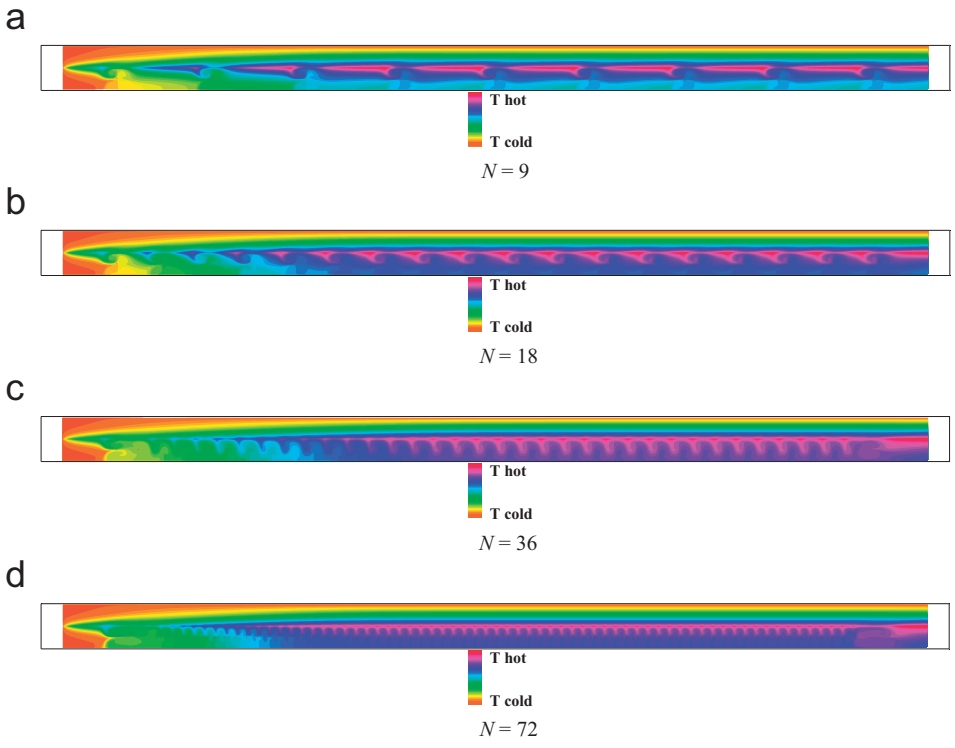

Fig. 10. Isotherm lines of various number of electrodes ($V_0 = 17.5\,\text{kV}$, $m_{Total} = 7.49\,\text{kg/hr}$, $m_U/m_{Total} = 50\%$, and $q = 1000\,\text{W/m}^2$).

the ratio less than 0.5 because the effect of placing electrodes at the lower channel performs the better heat transfer performance than the upper channel. Nevertheless, the EHD and non-EHD values are approach to be resembled at high mass flux because the effect of electric field is dominated by the effect of inlet velocity.

The effect of number of electrodes is represented in Fig. 11. Collector efficiency is significantly influenced with the number of electrodes, the trend of curve increases rapidly when the number is augmented and reaches the maximum point at the optimum number of electrodes as 18, but reduces due to the heat trap effect from many vortices as described in Fig. 4, when the number of electrodes is too high. The reason of this phenomena can be described by considering the ratio of distance between wire electrodes and distance of sub-channel height, the maximum point occurs when this value immediately approach one. The electric field from each wire electrode emanates from a point charge symmetrically in all directions. Field lines begin on positive (wire electrode) and end on negative (grounded plate), they cannot simply terminate in computational domain. Thus, at this ratio, it may be advantage

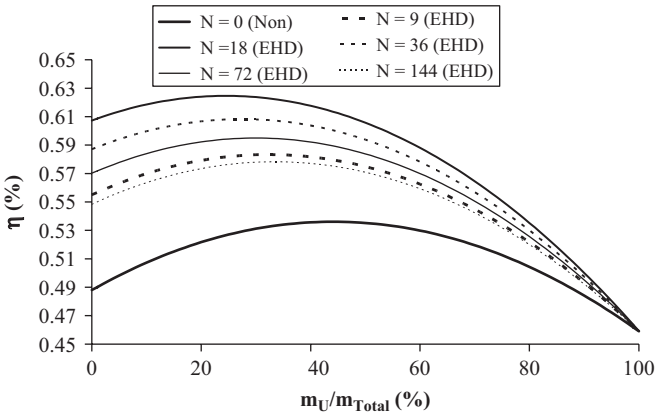

Fig. 11. Collector efficiency with different numbers of electrodes ($V_0 = 17.5\,\text{kV}$, $m_{Total} = 7.49\,\text{kg/h}$, and $q = 1000\,\text{W/m}^2$).

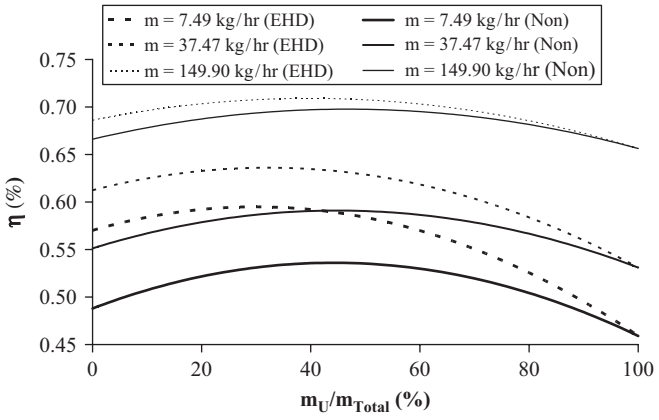

Fig. 12. Effect of total mass flux to the thermal efficiency ($V_0 = 17.5\,\text{kV}$, $N = 18$, and $q = 1000\,\text{W/m}^2$).

for polarization of ionic wind to the grounded plate. To verify that heat transfer enhancement is not due to the turbulent increment from the surface roughness of electrodes, the numerical test is done by including the wire electrodes that have diameter of $1 \times 10^{-4}\,\text{m}$ ($N = 72$ as same as in Fig. 9(d)) into the computational domain for non-EHD category and varying m_{Total} inside solar air heater from 7.49 to 149.90 kg/h. It is found that the increased collector efficiency in term of $(\eta_{\text{with electrode}}-\eta_{\text{without electrode}})100/\eta_{\text{without electrode}}$ is varied between 0.07% and 0.22% at $V_0 = 0\,\text{kV}$, $m_U/m_{Total} = 50$ %, and $q = 1000\,\text{W/m}^2$. These simulation results of non-EHD effect are also compared with the previous experimental study [11] that agrees quite well. Moreover, the effect of friction loss (from shear and normal forces) increased due to the adding electrodes is also determined at the same configuration. The calculated results show that the augmented pressure drop between inlet and outlet is in the range of 1.48–2.40% compared with those of no electrode installed inside channel, which found to be decline significantly because its area is small in a comparison with the total wall area. Fig. 12 investigates the effect of total mass flux to the collector efficiency. It can

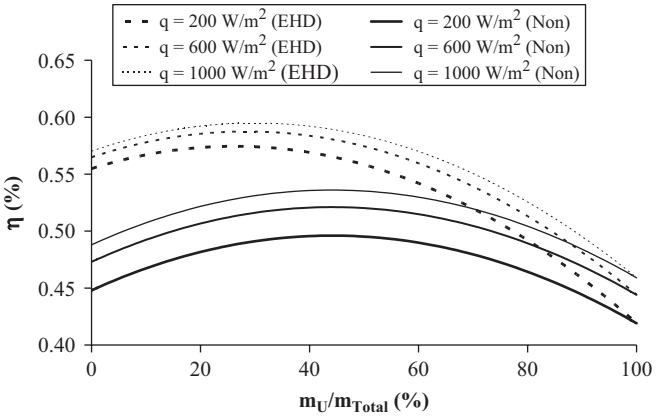

Fig. 13. Effect of heat flux at an absorbing plate to the thermal efficiency ($V_0 = 17.5\,\text{kV}$, $N = 18$, and $m_{Total} = 7.49\,\text{kg/h}$).

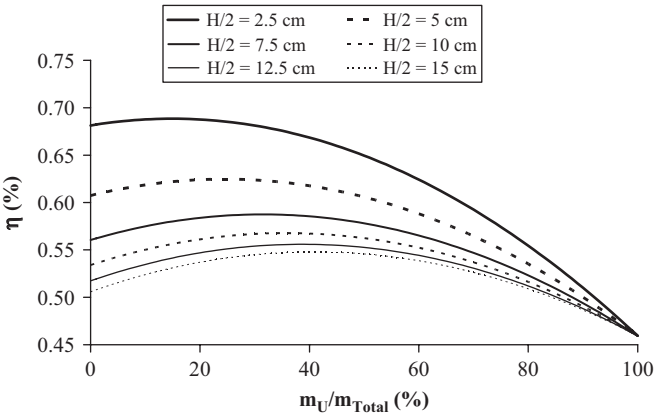

Fig. 14. Collector efficiency with different channel heights ($V_0 = 17.5\,\text{kV}$, $N = 18$, $m_{Total} = 7.49\,\text{kg/h}$, and $q = 1000\,\text{W/m}^2$).

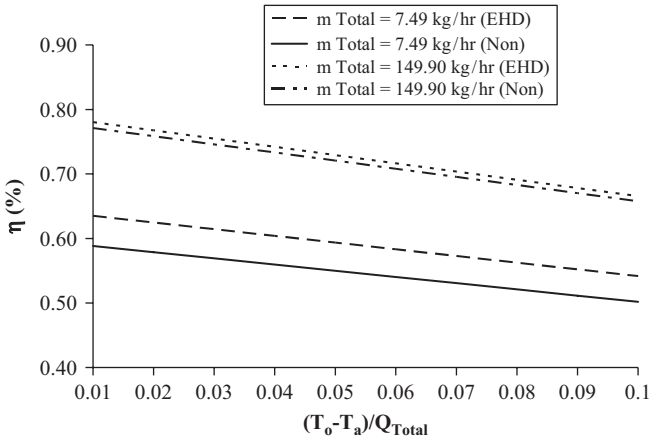

Fig. 15. Collector efficiency related to outlet temperature of each total mass flux ($V_0 = 17.5\,\text{kV}$, $N = 18$, $m_U/m_{Total} = 50\%$, and $q = 1000\,\text{W/m}^2$).

be observed that at low mass flux has more augmented ratio than high mass flux. Fig. 13 shows the effect of total heat flux to the collector efficiency, the heat transfer enhancement is more significant at lower heat flux. The increase of absorbing plate heat flux causes the significant resistance of the flow characteristic, thus EHD is

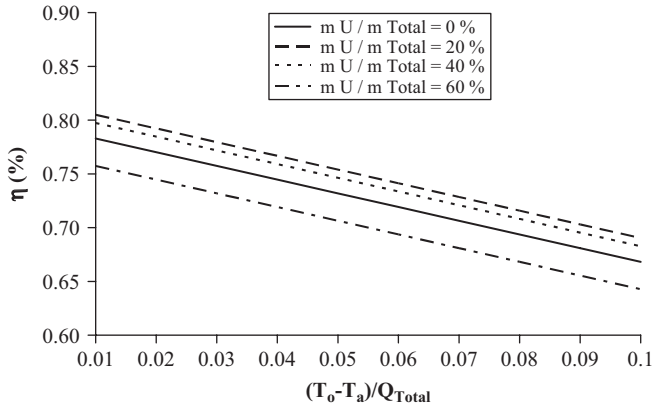

Fig. 16. Collector efficiency related to outlet temperature of each mass flux ratios ($V_0 = 17.5$ kV, $N = 18$, $m_{Total} = 7.49$ kg/h, and $q = 1000$ W/m^2).

dominated by primary flow in this phenomenon. Fig. 14 indicates the effect of channel height; more electric field strength at low channel height yields high collector efficiency. These simulation results of the optimum mass flux ratio of electrode arrangement guarantee that the suitable ratio is obtained between 20% and 30% for all operating conditions. The thermal efficiency curves as a function of the difference between outlet and ambient temperature are finally represented in Figs. 15 and 16 that confirm the previous results. It is in direct relation to the efficiency and the mass flux that can be calculated based on various inlet temperatures. When designing solar air heater, it is often useful to know which temperature level can be expected out of the collector.

5. Conclusion

The conclusions obtained are as follows:

The flow pattern of fluid flow is affected with the supplied voltage. The enhancement of heat transfer coefficient with the presence of an electric field increases with the supplied voltage but decreases with the total mass flux. Electrode installation at lower channel performs the best collector performance for double-flow solar air heater. The collector efficiency increases to the maximum at the optimized number of electrodes, which has ratio between electrode distance and sub-channel height at one. A channel height also influences the collector efficiency, lower height gives more strength to the electric field, which results in better thermal performance. The optimum mass flux ratio between upper and total is found to be approximately between 20% and 30%.

Acknowledgement

The authors gratefully acknowledge the support provided by the Thailand Research Fund and Commission on Higher Education for carrying out this study.

References

[1] Satcunanathan S, Deonarine SA. Two-pass solar air heater. Sol Energy 1973;15:41–9.
[2] Wijeysundera NE, Ah LL, Tjioe LE. Thermal performance study of two-pass solar air heaters. Sol Energy 1982;28:363–70.
[3] Yeh HM, Ho CD, Hou JZ. The improvement of collector efficiency in solar air heaters by simultaneous air flow over and under the absorbing plate. Energy 1999;24:857–71.
[4] Yeh HM, Ho CD, Hou JZ. Collector efficiency of double-flow solar air heaters with fins attached. Energy 2002;27:715–27.
[5] Yabe A, Mori Y, Hijikata K. EHD Study of the corona wind between wire and plate electrodes. AIAA J 1978;16:340–5.
[6] Velkoff HR, Godfrey R. Low velocity heat transfer to a flat plate in the presence of a corona discharge in air. J Heat Transfer 1979;101:157–63.
[7] Yamamoto T, Velkoff HR. Electrohydrodynamics in an electrostatic precipitator. J Fluid Mech 1981;108:1–18.
[8] Tada Y, Takimoto A, Hayashi Y. Heat transfer enhancement in a convective field by applying ionic wind. J Enhanced Heat Transfer 2002;4:71–86.
[9] Kasayapanand N, Tiansuwan J, Asvapoositkul W, Vorayos N, Kiatsiriroat T. Effect of the electrode arrangements in tube bank on the characteristic of electrohydrodynamic heat transfer enhancement: low Reynolds number. J Enhanced Heat Transfer 2002;9:229–42.
[10] Kasayapanand N, Kiatsiriroat T. EHD enhanced heat transfer in wavy channel. Int J Commun Heat Mass Transfer 2005;32:809–21.
[11] Kasayapanand N, Kiatsiriroat T. Optimized electrode arrangement in solar air heater. Renew Energy 2006;31:439–55.
[12] Landau LD, Lifshitz EM. Electrohydrodynamics of continuous media. New York: Pergamon; 1963.
[13] Lami E, Mattachini F, Sala R, Vigl H. A mathematical model of electrostatic field in wires-plate electrostatic precipitators. J Electrostat 1997;39:1–21.
[14] Talaie MR, Taheri M, Fathikaljahi J. A new method to evaluate the voltage–current characteristics applicable for a single-stage electrostatic precipitator. J Electrostat 2001;53:221–33.
[15] Anagnostopoulos J, Bergeles G. Corona discharge simulation in wire-duct electrostatic precipitator. J Electrostat 2002;54:129–47.
[16] Peek FW. Dielectric phenomena in high-voltage engineering. New York: McGraw-Hill; 1929.